Contribution from the Chemistry Department,
Kuwait University, Box 5969, 13060 Safat, Kuwait

Theoretical Study of the Bonding in Sulfur- and Oxygen-Containing Molybdenum Species of the General Formula $MoS_nO_{4-n}^{2-}$ (n = 0–4)

B. D. El-Issa,* A. A. M. Ali, and H. Zanati

Received September 29, 1988

In this paper, we present a comparative study of the class of molybdenum compounds of the formula $MoS_nO_{4-n}^{2-}$ (n = 0–4). The tetrathio speices is known to be of bioinorganic importance that can undergo ligand-exchange processes in aqueous solution in which a sulfur ligand is replaced by an oxygen counterpart. The study discusses the bonding properties in these compounds under different symmetry environments. Certain conclusions are drawn as to the type of bonds that are expected to develop between the central molybdenum atom and the ligand orbitals. Transition energies and ionization potentials are also discussed.

Introduction

Chalcogen–metal complexes and chalcogenometalates in which the central atom is either Mo or W in a d^0 configuration have been recently reported to be of special importance as bioinorganic agents.[1-4] Extensive studies have been conducted in aqueous media of the respective salts of these species. There is now growing evidence that species of the form MS_4^{2-} (M = Mo, W) can undergo ligand-exchange process in aqueous solution that will successively lead to an interchange of the oxygen and sulfur ligands.[5,6] Chalcogenometalate species of the general formula $MoS_nO_{4-n}^{2-}$ (n = 0–4) have therefore been correctly identified in solution, and various mechanisms have been suggested for their reactions. The type and the amount of bonding have been studied spectroscopically[7-11] and theoretically,[12-16] and very interesting features have been reported regarding the amount of the covalency in the bonds between the central metal and the sulfur and/or the oxygen ligands. Acceptor and donor orbitals have also been identified, and various computational methods have been conducted on the tetrachalcogen species. Experimental ionization energies, visible absorption techniques, and magnetic dichroism measurements[17,18] have all supported the theoretical assignment of the HOMO–LUMO excitation and have identified this to be a charge-transfer process from the ligand moieties to the central metal. Although this seems to be comprehensive, few studies have actually dealt with proposing a unified theoretical model that will attempt to elaborate on the electronic structure, the bonding properties, and the charge-transfer processes that involve species that are obtained as a result of the successive substitution of the sulfur ligands with oxygen counterparts.

In this study, we shall attempt to present such a model. It will perhaps be necessary to start by visualizing the central metal ion as a charged Mo^{6+} species surrounded by four ligand moieties situated at large distances in a tetrahedral environment. These ligand moieties are then made to approach the central ion at the respective equilibrium distance(s). Accordingly, the degeneracy of the central metal d orbitals and the s and p orbitals of the ligand moieties will be expected to be lifted in such a manner that will allow maximum overlap interactions between the central metal and the ligand moieties according to the respective symmetry types of the resulting molecular orbitals. The amount of σ and π interactions and the net charge on the metal and the corresponding ligand moities may thus be computed and comparatively studied.

Table I. Resolution of the Valence Molecular Orbitals under Different Symmetry Types in the Tetrathiomolybdenum Species

T_d	C_{3v}	C_{2v}	descripn of orbital in T_d sym
2e	6e	$3a_2$	LUMO, Mo(d) character, π-antibonding interactions
		$7a_1$	
$1t_1$	$1a_2$	$2a_2$	HOMO, S(p) character, weak π interactions
	5e	$4b_1$	
		$4b_2$	
$3t_2$	$5a_1$	$6a_1$	S(p), weak π interactions
	4e	$3b_1$	
		$3b_2$	
$2a_1$	$4a_1$	$5a_1$	Mo(s), S(p), weak π interactions
1e	3e	$4a_1$	Mo(d), S(p), π-bonding interactions
		$1a_2$	
$2t_2$	$3a_1$	$3a_1$	Mo(d), S(p), σ-bonding interactions
	2e	$2b_1$	
		$2b_2$	
$1t_2$	2a	$2a_1$	S(s), localized 3s orbitals
	1e	$1b_1$	
		$1b_2$	
$1a_1$	$1a_1$	$1a_1$	S(s), localized 3s orbitals

It is obvious, for instance, that a net charge of less than +6 on the Mo ion would indicate the amont of prevalent covalent character and, likewise, the coefficients in the linear expansion of the molecular orbitals that pertain to the E and T_2 irreducible representations should give an insight into the type of bonding that will dominate as a result of the interaction. Although the central metal d orbitals are not resolved into the same irreducible representations under the different symmetry types, one can still draw out certain correlations regarding the type of bonding that will be involved. For instance, the local $d_{x^2-y^2}$ and d_{z^2} orbitals of the central metal will be doubly degenerate in a tetrahedral environment but will be resolved into two singly degenerate orbitals in a C_{2v} environment. In a pure tetrahedral environment as in the case of MoS_4^{2-} and MoO_4^{2-}, the d^0 configuration on the Mo signifies that both the e and t_2 orbitals are initially empty. In the bond-formation process, however, any charge that develops on the Mo atom in occupied molecular orbitals that pertain to the E and T_2 irreducible representations must be interpreted as charge donated from the ligand moieties to the central Mo atom. The charge that develops on the Mo sphere in the 1e orbital, for instance, represents the amount of charge donated from the S or O moieties in order to form a bonding π orbital. One can also study the absorption bands that develop as the tetrathio anion is sequentially changed to the tetraoxo counterpart. This gradual

(1) Clark, N. J.; Laurie, S. H. *J. Inorg. Biochem.* **1980**, *12*, 37.
(2) Coughlan, M. P. *Molybdenum and Molybdenum Containing Enzymes*; Pergamon Press: New York, 1980.
(3) Burgmayer, S. J. N.; Stiefel, E. I. *J. Chem. Educ.* **1985**, *62*, 943.
(4) Müller, A.; Diemann, E.; Jostes, R.; Bogge, H. *Angew. Chem., Int. Ed. Engl.* **1981**, *20*, 934.
(5) Diemann, E.; Müller, A. *Coord. Chem. Rev.* **1973**, *10*, 79.
(6) Vogler, A.; Kunkely, H. *Inorg. Chem.* **1988**, *27*(3), 504.
(7) Müller, A.; Jørgensen, C. K.; Diemann, E. *Z. Anorg. Allg. Chem.* **1972**, *391*, 38.
(8) Clark, R. J. H.; Dines, T. J.; Wolf, M. L. *J. Chem. Soc., Faraday Trans. 2* **1982**, *78*, 679.
(9) Müller, A.; Diemann, E. *J. Chem. Phys.* **1974**, *61*(12), 5469.
(10) Bartecki, A.; Dembicka, D. *Inorg. Chim. Acta* **1973**, *7*(4), 610.
(11) Clark, R. J. H.; Walton, J. R. *J. Chem. Soc., Dalton Trans.* **1987**, 1535.
(12) Kebabcioglu, R.; Müller, A. *Chem. Phys. Lett.* **1971**, *8*, 59.
(13) Kebabcioglu, R.; Müller, A.; Rittner, W. *J. Mol. Struct.* **1971**, *9*, 207.
(14) Sasaki, T. A.; Kiuchi, K. *Chem. Phys. Lett.* **1981**, *84*(2), 356.
(15) Onopko, D. E.; Titov, S. A. *Opt. Spectrosc. (Engl. Transl.)* **1979**, *47*(2), 185.
(16) Müller, H.; Opitz, C.; Seifert, G. *Z. Phys. Chem.* **1981**, *262*(5), 1073.
(17) Liang, K. S.; Bernholc, J.; Pan, W. H.; Hughes, G. J.; Stiefel, E. I. *Inorg. Chem.* **1987**, *26*(9), 1422.
(18) Petit, R. H.; Briat, B.; Müller, A.; Diemann, E. *Mol. Phys.* **1974**, *27*(5), 1373.

0020-1669/89/1328-3297$01.50/0

Chart I

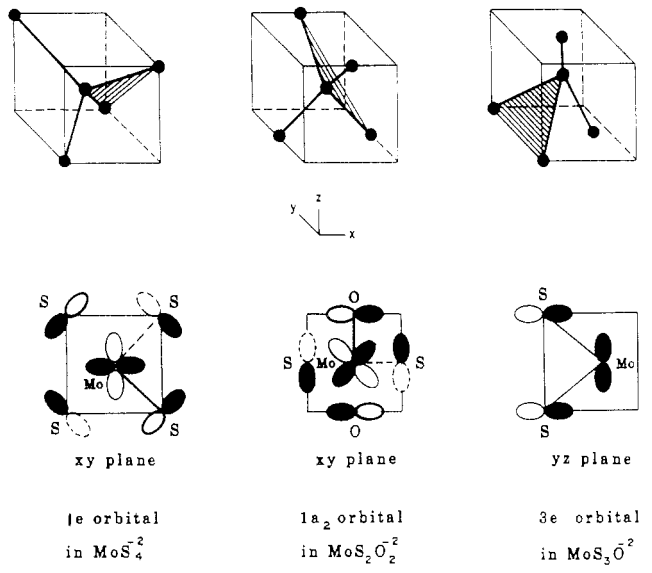

substitution of the S ligands by O counterparts would result in a change in symmetry from T_d to C_{3v}, C_{2v}, C_{3v}, and then finally T_d. Since both the C_{3v} and C_{2v} symmetry groups are subgroups of T_d, we shall find it useful to make a correlation of the transformed orbitals in a certain symmetry to their corresponding T_d resolvents. In Table I we show a typical bonding scheme in MoS_4^{2-}, the transformed orbitals under the C_{3v} and C_{2v} point symmetry groups, and the description of these orbitals. Chart I shows the relative position of the ligands in the different symmetry types. The formation of σ bonds between the ligand p orbitals and the Mo d or s orbitals is straightforward, but the formation of π bonds is less obvious. The shaded areas in Chart I represent the planes that contain the π bond. Projections in the *xy* and *yz* planes are also displayed. In these projections the broken contours represent ligand p orbitals below the Mo atom while solid contours represent such orbitals above the Mo atom. (For clarity, the oxygen p orbtial in MoS_3O^{2-} is intentionally deleted from the diagram.) Sections that contain the π bonds are also shown in the diagram. We note that, in the T_d symmetry type, the π bond will be associated with the Mo $d_{x^2-y^2}$ component while, in the case of $MoS_2O_2^{2-}$, it will be associated with the d_{xy} component of Mo. In the 3e orbital of MoS_3O^{2-} one expects to find the π bond in a plane that contains the Mo and the two sulfur atoms that lie on the same side of Mo. The difficulty in identifying the π bond in C_{3v} symmetry is because the *z* axis is taken conventionally to be coincident with the 3-fold rotational axis. This forces the three sulfur ligands to be contained in a trigonal plane. The construction of the 3e orbital in MoS_3O^{2-} and the 1e orbital in MoS_4^{2-} with the proper orthogonality requirements may be obtained from the respective projection operators defined by the appropriate irreducible representations. The orthogonal partner of the 3e orbital in MoS_3O^{2-} and the $4a_1$ orbital in $MoS_2O_2^{2-}$ are obviously counterparts to the orthogonal partner of 1e in MoS_4^{2-} that represents π interactions involving the Mo d_{z^2} components. This confusion is related to the fact that the conventional orientations of the ligand moieties are different in the three different symmetry types under study. In fact, the E irreducible representation does not span the same linear combination of d bases around the central atom in the tetrahedral and trigonal environments. In the case of a C_{2v} environment, however, the e orbitals transform as $a_1 + a_2$.

Method

The present work employs the use of the multiple scattering Xα (MS–Xα) theory[19,20] in generating a self-consistent field potential. The theory employs two important assumptions, namely a muffin tin like potential and an exchange potential that is proportional to the cube root of the charge density.[21] The method had been shown to be quite successful in interpreting the molecular structure of transition-metal complexes,[22-24] although the use of nonrelativistic corrections had been generally criticized for systems containing heavy elements ($Z > 35$).

For a central-field problem, the Schrödinger equation (in atomic units) takes the form

$$\left[-\frac{\partial^2}{\partial r^2} + \frac{l(l+1)}{r^2} + V(r) + V_{x\alpha}\right]R_{nl} = \epsilon_{nl}R_{nl} \qquad (1)$$

where R_{nl} is the radial wave function, $V(r)$ is a spherically symmetrical potential, $V_{x\alpha}$ is the exchange potential, ϵ_{nl} is the energy, and l is the angular momentum quantum number. The difficulty in employing the above equation arises when one attempts to simulate a wave function that represents a heavy atom. In a manner similar to the work of Koelling and Harmon,[25] Wood and Boring[26] have introduced the mass–velocity, the Darwin, and the spin–orbit coupling terms in the expansion of the total Hamiltonian. Cowan and Griffin[27] have applied these approximations to the central-field problem. From the method of Wood and Boring, the spin–orbit coupling term may be ignored and the self-consistent radial term may be used to evaluate the molecular wave function (see Appendix in ref 24). This method is reported to yield a surprisingly good correlation with the exact Slater–Dirac method. In this work we have used the Wood and Boring approximation in generating the relativistic radial wave functions around Mo.

The various parameters used in the calculations for the $MoS_nO_{4-n}^{2-}$ ($n = 0$–4) anions are reported in Table II. In order to stabilize the anion, a Watson sphere[28] having a charge equal to +2 and a radius slightly greater than that of the outer sphere was made to surround the anions. The exchange α values employed around the different atomic spheres were set equal to the Schwarz values,[29] whereas weighted averages in the inner- and outer-sphere regions were used. The sphere radii were calculated by using the criteria of Norman,[30] where the choice of the radii is made by enclosing the atomic number of electrons in the spherical regions and at the same time requiring satisfaction of the virial theorem. The percent sphere overlap was determined by choosing a factor of 0.88 of the atomic radii (Table II). In all the species studied, $l_{max} = 2$ was employed around the Mo atom, which corresponds to the truncation of the partial wave expansion at the d functions. The expansion around the outer sphere and the ligands (either oxygen or sulfur) was, however, truncated at the f and p functions, respectively. The threshold for the convergence of the potential was set equal to 10^{-5} in all the complexes.

Table II. Interatomic Distances, Sphere Radii (in au), and the α Exchange Values for the Different Molybdenum Species[a]

	MoS_4^{2-}	MoS_3O^{2-}	$MoS_2O_2^{2-}$	$MoSO_3^{2-}$	MoO_4^{2-}
α param for outer sphere	0.720	0.724	0.728	0.732	0.736
sphere radius of Mo	2.464	2.335	2.263	2.204	2.171
sphere radius of S	2.564	2.540	2.565	2.556	
sphere radius of O		1.796	1.794	1.791	1.803
sphere radius of outer sphere	6.705	7.401	6.707	8.539	5.035
sphere radius of Watson sphere	6.770	7.470	6.780	8.620	5.085
% overlap between Mo and S spheres	21.0	18.5	16.0	15.6	

[a] For all compounds, the maximum azimuthal quantum number was taken as follows: l_{max}(outer sphere) = 3; l_{max}(Mo) = 2; l_{max}(S) = 1; l_{max}(O) = 1. The Mo–S distance was taken as 4.117 bohr, and the Mo–O distance was taken as 3.214 bohr.

(19) (a) Slater, J. C. *J. Chem. Phys.* **1965**, *43*, S228. (b) Slater, J. C. *Quantum Theory of Molecules and Solids*; McGraw-Hill: New York, 1974; Vol. IV.

(20) (a) Johnson, K. H. *J. Chem. Phys.* **1966**, *45*, 3085. (b) Johnson, K. H. *Int. J. Quantum Chem.* **1967**, *1S*, 361. (c) Johnson, K. H. *Int. J. Quantum Chem.* **1971**, *4*, 153. (d) El-Issa, B. D. *Int. J. Quantum Chem.* **1981**, *S15*, 419.
(21) Johnson, K. H. *Adv. Quantum Chem.* **1973**, *7*, 143.
(22) Goursot, A.; Chermette, H. *Can. J. Chem.* **1985**, *63*, 1407.
(23) El-Issa, B. D.; Katrib, A.; Ghodsian, R.; Salsa, B. A.; Adassi, S. H. *Int. J. Quantum Chem.* **1988**, *33*, 195.
(24) El-Issa, B. D.; Makhyoun, M. A.; Salsa, B. A. *Int. J. Quantum Chem.* **1987**, *31*, 295.
(25) Koelling, D. D.; Harmon, B. N. *J. Phys. C* **1977**, *10*, 3107.
(26) Wood, J. H.; Boring, A. M. *Phys. Rev. B* **1978**, *18*, 2701.
(27) Cowan, R. D.; Griffin, D. C. *J. Opt. Soc. Am.* **1976**, *66*, 1010.
(28) Watson, R. E. *Phys. Rev.* **1958**, *111*, 1108.
(29) Schwarz, K. *Phys. Rev. B* **1972**, *B5*, 2466.
(30) (a) Norman, J. G., Jr. *J. Chem. Phys.* **1974**, *61*, 4630. (b) Norman, J. G., Jr. *J. Mol. Phys.* **1976**, *31*, 1191.

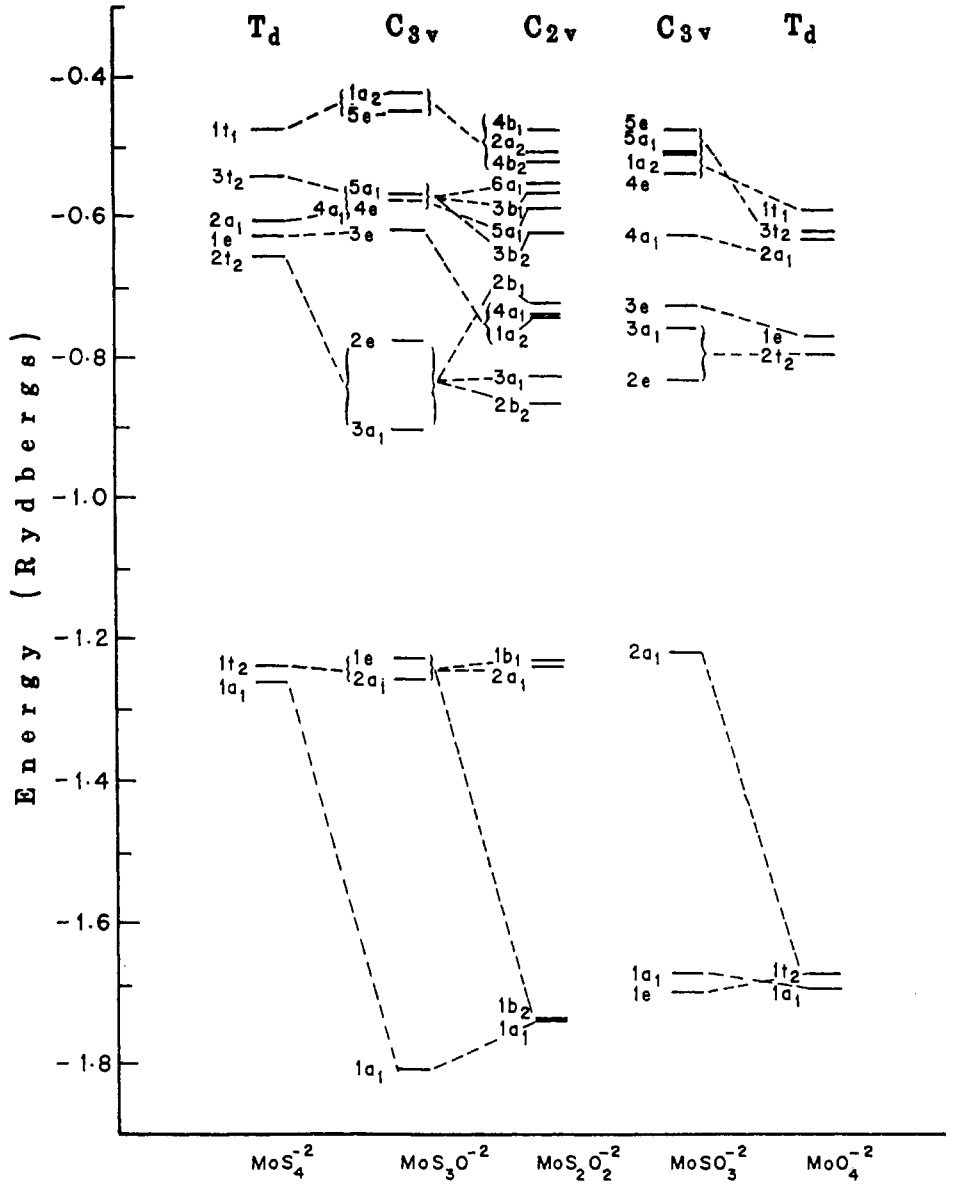

Figure 1. Correlation diagram that shows the MS–Xα orbital energies (in rydbergs) of the different molybdenum species according to the various symmetry types.

The ionization energies were calculated by removing half an electron from the respective orbital of the converged system and then iterating for a new self-consistency in the resulting potential.[31] In a similar manner, the transition-state energies were calculated by promoting half an electron from the required orbital in the ground state to the desired empty orbital.

Results and Discussion

In Tables III–VI we report the MS–Xα orbital energies in rydbergs and their respective charge compositions for the thiomolybdenum species, in which the molecular orbitals are referred to the relevant symmetry group notation. In Table VII we report similar data for the MoO_4^{2-} anion. In the discussion that follows, we shall attempt to correlate the molecular orbitals in a low-symmetry species with the corresponding orbitals in tetrahedral symmetry. This descent-in-symmetry approach will prove useful in describing the transformation of the orbitals as one goes from high to low symmetry. The transformed orbitals, however, will not preserve the same orthogonality requirements and will be represented by different bonding schemes. In a T_d environment, for instance, the E irreducible representation will represent π interactions with the sulfur or oxygen moieties, but orbitals that transform under the same irreducible representation in a C_{3v} environment will constitute pseudo π interactions, as will be made evident in the case of the trithio- and monothiomolybdate species. Table VIII is a correlation table that displays the transformed orbitals and their MS–Xα energies under the respective symmetry types, while Figure 1 is a correlation diagram that shows the relative positions of the transformed orbitals. The orbitals displayed in Table VIII are arranged in descending order with respect to the orbital energies of the tetrathio species.

In studying the electronic structure of MoS_4^{2-} (Table III), it

Table III. Molecular Orbital Energies (in rydbergs) and Charge Composition of the Respective Molecular Orbitals in MoS_4^{2-} in a Tetrahedral Environment[a]

molecular orbital	orbital energy	Mo			S	
		s	p	d	s	p
$4t_2$	−0.152		0.157	0.474		0.088
2e*	−0.289			0.716		0.071
$1t_1$	−0.472					0.250
$3t_2$	−0.545		0.072	0.005		0.230
$2a_1$	−0.605	0.193			0.006	0.196
1e	−0.627			0.340		0.165
$2t_2$	−0.656		0.008	0.398	0.003	0.146
$1t_2$	−1.239		0.025	0.054	0.229	0.001
$1a_1$	−1.261	0.072			0.230	0.002

[a] The LUMO is indicated by an asterisk.

(31) Slater, J. C. *Adv. Quantum Chem.* **1972**, *6*, 1.

Table IV. Molecular Orbital Energies (in rydbergs) and Charge Composition of the Respective Orbitals of MoS_3O^{2-} in a C_{3v} Environment[a]

molecular orbital	orbital energy	Mo			O		S	
		s	p	d	s	p	s	p
$6a_1$	−0.196	0.276	0.312	0.231		0.051	0.04	
6e*	−0.300		0.006	0.717		0.043		0.077
$1a_2$	−0.422							0.333
5e	−0.447		0.002	0.021		0.030		0.315
$5a_1$	−0.566		0.066			0.065		0.287
4e	−0.577		0.041	0.076		0.188		0.231
$4a_1$	−0.578	0.148	0.013	0.031		0.003	0.002	0.266
3e	−0.619		0.010	0.373		0.041		0.191
2e	−0.776			0.273		0.570	0.004	0.047
$3a_1$	−0.903	0.020	0.022	0.287	0.024	0.615	0.002	0.009
1e	−1.225		0.015	0.063		0.003	0.305	
$2a_1$	−1.255	0.040	0.017		0.003	0.004	0.310	0.002
$1a_1$	−1.808	0.024	0.053	0.078	0.834	0.005		

[a] The LUMO is indicated by an asterisk.

Table V. Molecular Orbital Energies (in rydbergs) and Charge Composition of the Respective Orbitals of $MoS_2O_2^{2-}$ in a C_{2v} Environment[a]

molecular orbital	orbital energy	Mo			O		S	
		s	p	d	s	p	s	p
$3a_2$	−0.217			0.777		0.080		0.032
$7a_1$*	−0.227		0.016	0.759		0.052		0.060
$4b_1$	−0.489		0.002			0.022		0.477
$2a_2$	−0.506			0.014		0.077		0.416
$4b_2$	−0.521		0.013			0.056		0.438
$6a_1$	−0.552	0.028	0.039	0.029		0.030	0.002	0.420
$3b_1$	−0.567		0.048	0.143		0.107	0.002	0.295
$5a_1$	−0.587	0.111		0.085		0.048	0.003	0.350
$3b_2$	−0.620		0.036			0.459		0.022
$2b_1$	−0.723		0.004	0.260		0.288	0.002	0.078
$4a_1$	−0.739	0.025	0.023	0.229		0.335		0.026
$1a_2$	−0.744			0.274		0.328		0.034
$3a_1$	−0.827	0.024	0.005	0.292	0.004	0.323		0.010
$2b_2$	−0.865		0.020	0.328	0.008	0.312		0.006
$1b_1$	−1.228		0.016	0.042			0.470	
$2a_1$	−1.238	0.020	0.009	0.024			0.472	
$1b_2$	−1.735		0.060	0.088	0.425			
$1a_1$	−1.738	0.040	0.031	0.046	0.440			

[a] The LUMO is indicated by an asterisk.

Table VI. Molecular Orbital Energies (in rydbergs) and Charge Composition of the Respective Orbitals of $MoSO_3^{2-}$ in a C_{3v} Environment[a]

molecular orbital	orbital energy	Mo			O		S	
		s	p	d	s	p	s	p
$6a_1$	−0.115	0.017		0.098		0.193	0.234	
6e*	−0.163			0.794		0.059		0.025
5e	−0.481		0.006	0.005		0.050		0.837
$5a_1$	−0.506	0.001	0.075	0.074		0.076		0.620
$1a_2$	−0.510					0.333		
4e	−0.538		0.021	0.005		0.298		0.078
$4a_1$	−0.628	0.149	0.024	0.003		0.259	0.002	0.042
3e	−0.726			0.272		0.240		0.008
$3a_1$	−0.756	0.004	0.004	0.270		0.193	0.013	0.127
2e	−0.832		0.016	0.324	0.008	0.208		0.011
$2a_1$	−1.217	0.008	0.012	0.035		0.002	0.935	0.002
$1a_1$	−1.672	0.057	0.040		0.299		0.003	0.002
1e	−1.697		0.045	0.097	0.284	0.002		

[a] The LUMO is indicated by an asterisk.

will be important to consider the orbitals that constitute σ and π interactions between the Mo and the sulfur ligands. The LUMO is 2e and is unmistakably identified as a π^* orbital that is described by antibonding interactions between the Mo($d_{x^2-y^2}$) and the Mo(d_{z^2}) orbitals with the S(p) bases. Figure 2a shows a countour map that represents this orbital in a plotting plane that contains the Mo and two S ligands and is related to the Mo($d_{x^2-y^2}$) component, whereas Figure 2b shows a contour map that represents the degenerate counterpart of this orbital in a plotting plane taken at an angle of 45° from the *xy* plane and is related to the Mo(d_{z^2}) component. The bonding counterpart of this orbital is 1e (Figure 3) and represents π-bonding interactions between similar components of the Mo(d) orbitals and the S(p) functions. This orbital is of preponderant S(p) character and is a typical example of (a)

Table VII. Molecular Orbital Energies (in rydbergs) and Charge Composition of the Respective Molecular Orbitals in MoO_4^{2-} in a Tetrahedral Environment[a]

molecular orbital	orbital energy	Mo			O	
		s	p	d	s	p
2e*	−0.253			0.804		0.049
$1t_1$	−0.590					0.250
$3t_2$	−0.621		0.073	0.037		0.222
$2a_1$	−0.636	0.160				0.210
1e	−0.771			0.248		0.188
$2t_2$	−0.796		0.004	0.300		0.173
$1t_2$	−1.673		0.047	0.064	0.222	
$1a_1$	−1.694	0.064			0.234	

[a] The LUMO is indicated by an asterisk.

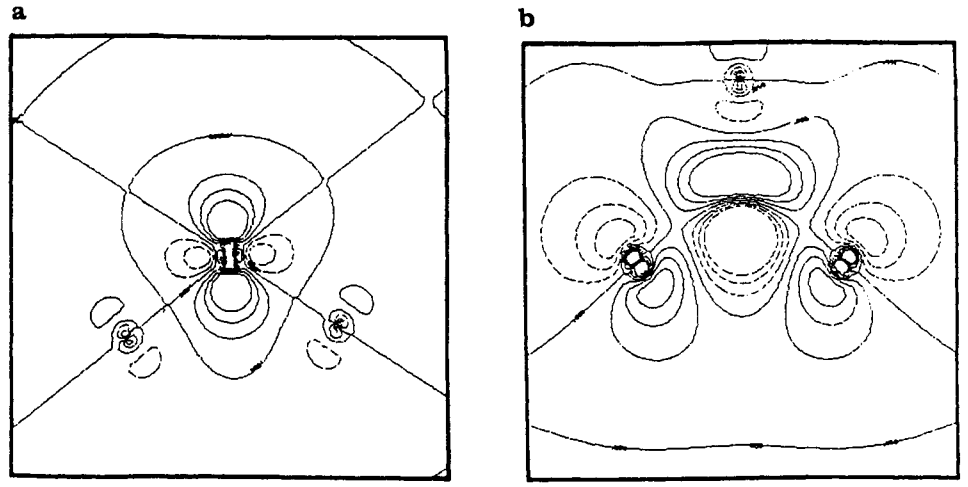

Figure 2. Contour maps of the doubly degenerate 2e orbital in MoS_4^{2-}. The plotting plane in part a contains Mo and two S ligands and shows antibonding interactions involving the Mo($d_{x^2-y^2}$) component. Part b is a countour map that shows antibonding interactions involving the Mo(d_{z^2}) component in a plane taken at 45° to the *xy* plane. Contour lines are taken from −0.3 to 0.3 with increments of 0.1.

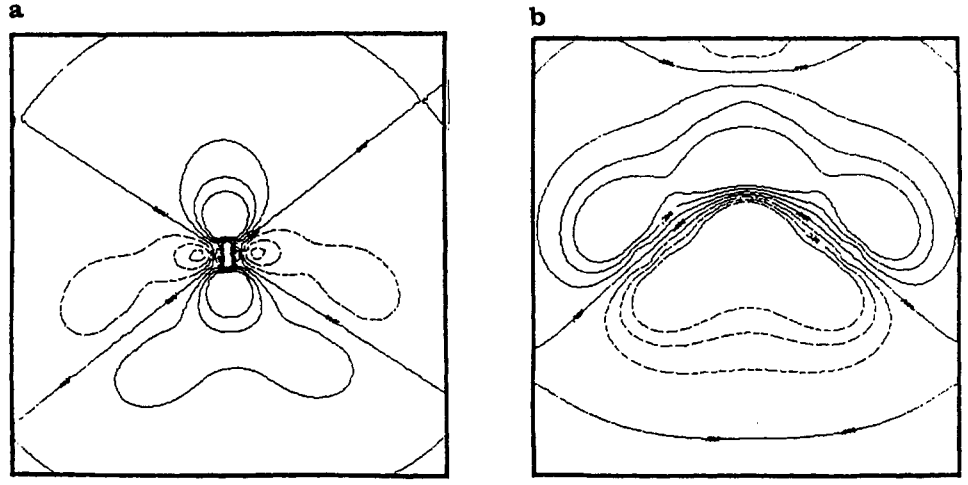

Figure 3. Contour maps of the 1e orbital in MoS_4^{2-}, which show π-bonding interactions between the Mo($d_{x^2-y^2}$) component the Mo(d_{z^2}) component (b) 3b) and ligand p orbitals. Plotting planes are similar to those in Figure 2, respectively. Increments of contour lines are the same as in Figure 2.

Table VIII. Transformed Orbitals and Orbital Energies (in rydbergs) of the Molybdenum Species in Their Respective Environments

MoS_4^{2-}	MoS_3O^{2-}	$MoS_2O_2^{2-}$	$MoSO_3^{2-}$	MoO_4^{2-}
$1t_1$ (−0.472)	$1a_2$ (−0.422) 2e (−0.447)	$4b_1$ (−0.489) $2a_2$ (−0.506) $4b_2$ (−0.521)	$1a_2$ (−0.510) 4e (−0.538)	$1t_1$ (−0.590)
$3t_2$ (−0.545)	$5a_1$ (−0.566) 4e (−0.577)	$6a_1$ (−0.552) $3b_1$ (−0.567) $3b_2$ (−0.620)	5e (−0.481) $5a_1$ (−0.506)	$3t_2$ (−0.621)
$2a_1$ (−0.605)	$4a_1$ (−0.578)	$5a_1$ (−0.587)	$4a_1$ (−0.628)	$2a_1$ (−0.636)
1e (−0.627)	3e (−0.619)	$4a_1$ (−0.739) $1a_2$ (−0.744)	3e (−0.726)	1e (−0.771)
$2t_2$ (−0.656)	2e (−0.776) $3a_1$ (−0.903)	$2b_1$ (−0.723) $3a_1$ (−0.827) $2b_2$ (−0.865)	$3a_1$ (−0.756) 2e (−0.832)	$2t_2$ (−0.796)
$1t_2$ (−1.239)	1e (−1.225) $2a_1$ (−1.255)	$1b_1$ (−1.228) $2a_1$ (−1.238) $1b_2$ (−1.735)	$2a_1$ (−1.217) 1e (−1.697)	$1t_2$ (−1.673)
$1a_1$ (−1.261)	$1a_1$ (−1.808)	$1a_1$ (−1.738)	$1a_1$ (−1.672)	$1a_1$ (−1.694)

π interactions that involve appropriate Mo(d) orbitals and the S(p) bases and (b) σ interactions between the S(p) bases. The HOMO is $1t_1$, and it represents weak π interactions between the S(p) orbitals and, for symmetry considerations, does not contain any Mo(d) character. The $3t_2$ orbital also contains preponderant S(p) character, while the $2a_1$ orbital represents σ interactions between the S(p) and Mo(s) bases. The $2t_2$ orbital is of special interest since it incorporates σ interactions between the Mo(d_{xz},d_{yz},d_{xy}) and the S(p) orbitals. Figure 4 shows a set of contour maps that shows these interactions in the *xz* and *yz* planes. The 3s orbitals of the sulfur groups according to this scheme are resolved into the triply degenerate $1t_2$ and the $1a_1$ orbitals. The longest wavelength transition that, obviously, involves a promotion of an electron from the $1t_1$ to the 2e orbitals is a singlet excitation of the type ($^1T_2 \leftarrow {}^1A_1$) and is a charge-transfer process. Excitation of electrons from the 1e and $1t_2$ orbitals to the LUMO is also of a type that involves charge transfer from the sulfur ligands to the central Mo ligand.

We now consider the bonding scheme in MoS_3O^{2-}, in which there is a descent in symmetry from T_d to C_{3v} (Table IV). In such an environment the nine sulfur p functions will be resolved into a 3E, $2A_2$, and A_1 set while the three p functions on the oxygen ligand will be resolved into an E and an A_1 set. Because of the relative positions of the p functions of free S and O, the molecular orbitals that will contain preponderant O(p) character will be expected to be lower in energy than those that contain preponderant S(p) character. It is also important to note that the HOMO will be a pure state that contains S(p) bases. Accordingly, the molecular orbitals will be arranged according to the following scheme: $1a_2$, 5e (S(p) character; counterpart to $1t_1$ in T_d symmetry); $5a_1$, 4e (S(p) character; counterpart to $3t_2$ in T_d symmetry); $4a_1$ (S(p) character; counterpart to $4a_1$ in T_d symmetry); 3e (S(p) character; counterpart to 1e in T_d symmetry); 2e, $3a_1$ (O(p) character; counterpart to $3t_2$ in T_d symmetry); 1e, $2a_1$ (S(s) character; counterpart to $1t_2$ in T_d symmetry); and $1a_1$ (O(s) character; counterpart to $1a_1$ in T_d symmetry). It is apparent that the 3e orbital in MoS_3O^{2-} does not transform in the same way as the 1e orbital in MoS_4^{2-}. In fact the 3e orbital contains an

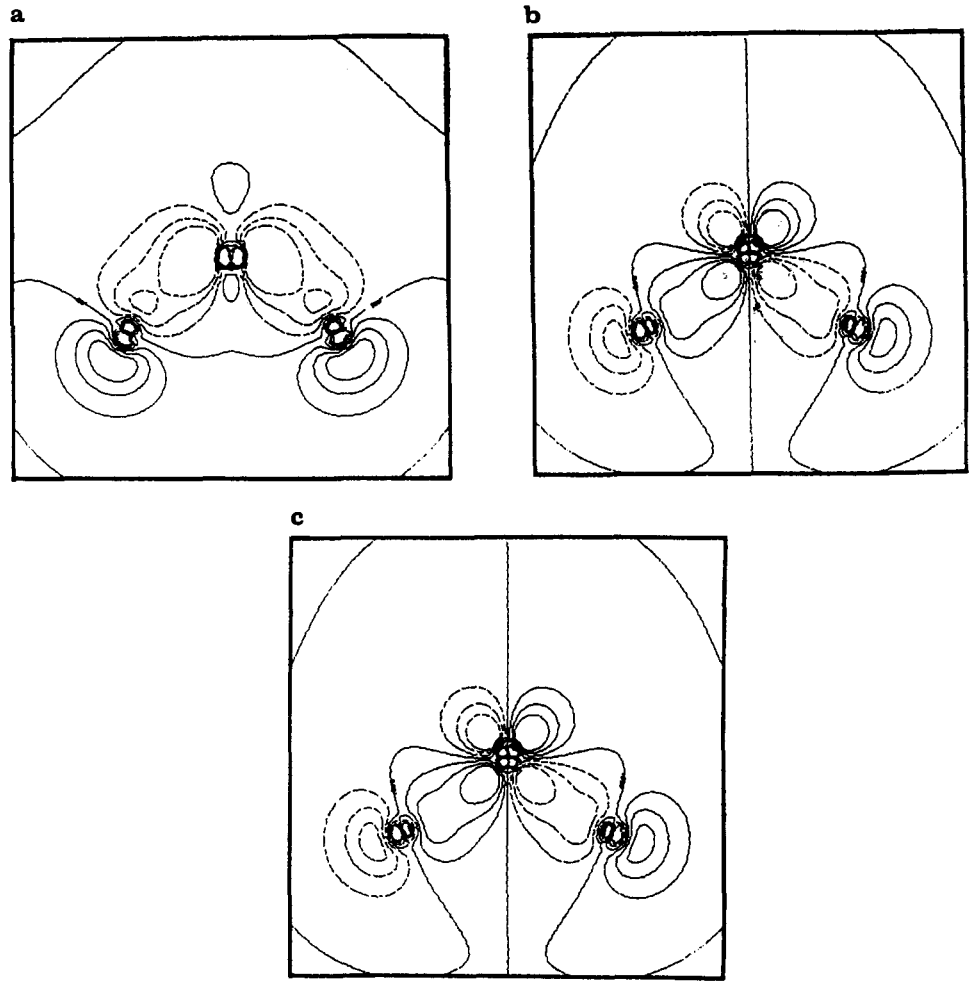

Figure 4. Contour maps of the triply degenerate $2t_2$ orbital in MoS_4^{2-} showing σ-bonding interactions involving the Mo(d_{xy}) component (a), the Mo(d_{xz}) component (b), and the Mo(d_{yz}) component (c) and ligand p orbitals. The maps are taken in sections that contain the Mo atom, two S ligands, and the z axis. Increments of contour lines are the same as in Figure 2.

admixture of σ and π interactions (a pseudo π type orbital) that involve the Mo(4d) basis, as may be verified by the contour maps shown in Figure 5. The bonding scheme in the 2e orbital is of special interest since it represents σ interactions that involve the S(p) and Mo(d) bases (Figure 6) and π interactions that involve the O(p) and the Mo(d) bases (Figure 6b). The LUMO in MoS_3O^{2-} is 6e, and the absorption band that corresponds to the longest wavelength involves a promotion of an electron from the $1a_2$ to the 6e orbital and is of the type $^1E \leftarrow {}^1A_1$.

We now consider the dithiomolybdate ion ($MoS_2O_2^{2-}$) in a C_{2v} environment (Table V). The occupied orbitals in this ion are all singly degenerate, and one expects to find six orbitals each of preponderant sulfur and oxygen p character and two orbitals each of preponderant sulfur and oxygen s character for a total of 16 occupied orbitals, which, because of symmetry, all contain admixtures of S, O, and Mo bases. We identify the electronic structure as follows: $4b_1$, $2a_2$, $4b_2$ (S(p) character; counterpart to $1t_1$ in T_d symmetry); $6a_1$, $3b_1$ (S(p) character), $3b_2$ (O(p) character) (counterpart to $3t_2$ in T_d symmetry); $5a_1$ (S(p) character; counterpart to $2a_1$ in T_d symmetry); $4a_1$, $1a_2$ (O(p) character; counterpart to 1e in T_d symmetry); $2b_1$, $3a_1$, $2b_2$ (O(p) character; counterpart to $2t_2$ in T_d symmetry); $1b_1$, $2a_1$ (S(s) character), $1b_2$ (O(s) character) (counterpart to $1t_2$ in T_d symmetry); $1a_1$ (O(s) character, counterpart to $1a_1$ in T_d symmetry).

An analysis of the composition of the orbitals reveals the fact that the oxygen ligands are more involved than the sulfur ligands in bonding with the Mo(d) basis and that such orbitals are consistently lower in energy than orbitals containing preponderant S(p) character. The only orbital that has predominant S(p) character and that is involved in bonding with the Mo(d) bases is $3b_1$, and it is characterized by σ interactions. In addition, one expects to find an orbital that involves π mixing similar to the 1e orbital in MoS_4^{2-}, which proved to be absent in a C_{3v} environment that lacks a C_2 axis of rotation. $1a_2$ is such an orbital, and it is depicted in the contour map of Figure 7. The LUMO in $MoS_2O_2^{2-}$ is $7a_1$ and as expected has predominant Mo(d) character.

In the monothiomolybdate ion ($MoSO_3^{2-}$), there is an important interchange of the set of orbitals that were previously associated with the $1t_1$ and $3t_2$ orbitals in MoS_4^{2-} (Table VI). This is not surprising since, in a C_{3v} environment, the three orbitals that contain predominant S(p) character are resolved under the appropriate unitary transformation into E + A_1 irreducible representations, which are expected to be higher in energy than the corresponding orbitals that contain O(p) character. The orbital that contains pure O(p) character ($1a_2$) is therefore shifted down in energy relvative to that of the $5a_1$ and 5e set that transforms in a proper tetrahedral environment to the $3t_2$ orbital (see Figure 1). Note that in Table VIII the $1a_2$ and 4e orbitals are not the highest occupied molecular orbitals. Their position in the table has been intentionally kept alongside the $1t_1$ orbital of the MoO_4^{2-} species.

We have by now demonstrated that, in the thiomolybdate species, the HOMO will consistently contain predominant sulfur p character irrespective of the amount of oxygen ligands present per formula unit. In cases where the thiomolybdate ions act as ligands in complexes that contain, for example, Fe or Cu, the HOMO will act as a donor orbital and consequently the sulfur ligands will be active in the bonding scheme of the complex. We also note that the oxygen ligands are more involved than the sulfur ligands in bonding with the Mo central ligand. Take for example the $3a_1$ and 2e orbitals in MoS_3O^{2-} and $MoSO_3^{2-}$. In both these cases, the respective orbitals have preponderant Mo(d) and O(p) character. This, however, should not be taken to mean that oxygen

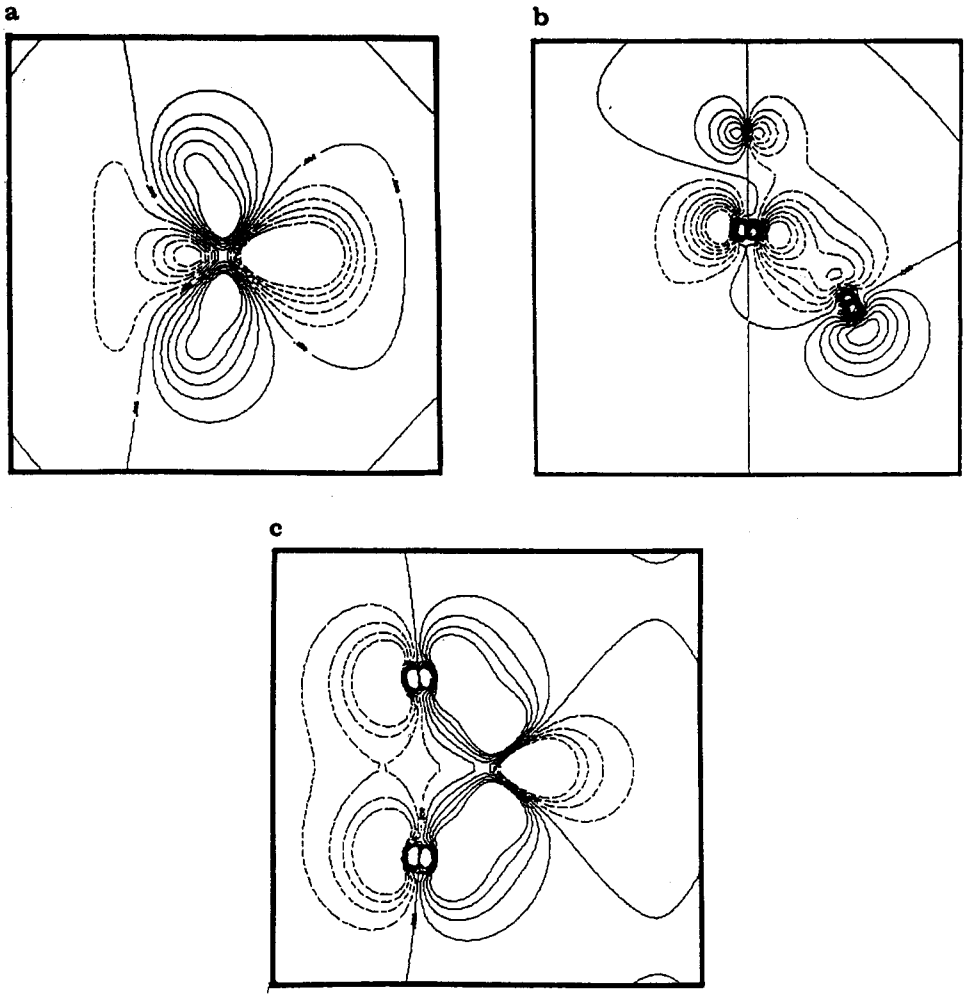

Figure 5. Contour maps of the 3e orbital in $MoS_3O_2^-$ that show pseudo π interactions involving the Mo(4d) and the S(p) functions. The section in part a is in the xy plane and shows the Mo(4d) orbital in a C_{3v} environment. The section in part b is taken in the xz plane, while that in part c is taken in a plane that contains the Mo atom and the two S ligands that lie on the two corners of the cube (see Chart I). Contour lines are taken from −0.2 to 0.2 to increments of 0.05.

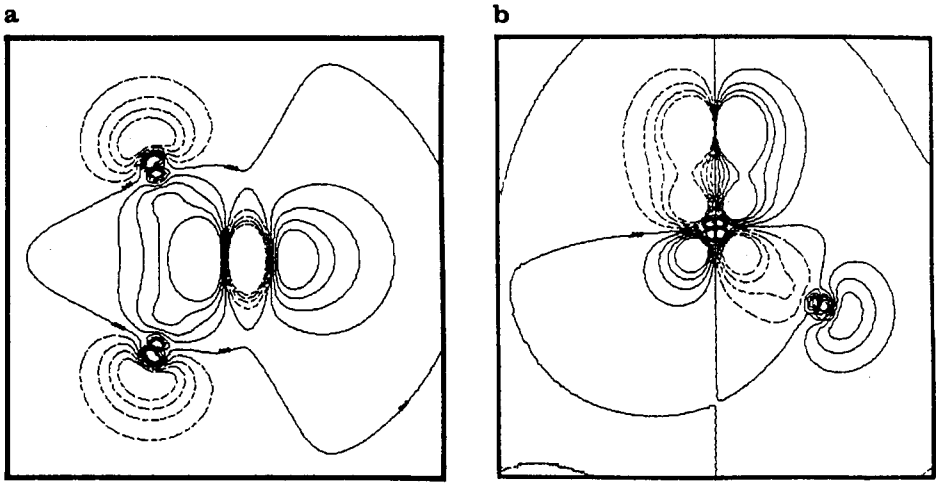

Figure 6. Contour maps of the 2e orbital in MoS_3O^{2-} showing σ interactions involving the Mo(d_{xz}) component and S(p) functions. The plotting plane in part a is taken in a section that contains the Mo and two S ligands (Chart I), while that in part b is taken in the xz plane. Increments of contour lines are the same as in Figure 5.

ligands are better electron donors than sulfur ligands. In fact our results show that the contrary is the case. The net amount of donation should be computed by multiplying the charge on, for example, the d component of Mo in a given molecular orbital by the occupany of that orbital and then summing over all the occupied orbitals. We do this for the Mo(d) component, and we find for the series $MoS_nO_{4-n}^{2-}$ that the net amount of charge donation (to the Mo(d) component) is 4.8, 4.0, 3.7, 3.6, and 3.4 for n = 4–0, respectively. One explanation is perhaps due to the fact that the oxygen p orbitals, under the different symmetry types, are resolved into a set that transforms to the $2t_2$ orbital in T_d symmetry and are thus ideal for interaction with the Mo(d) orbitals that have acquired most of their charge from the S ligands. The fact that the sulfur ligands are better electron donors (i.e. have more reducing power) than the oxygen ligands may be deduced readily by inspecting the composition of the 1e, $2t_2$, and $2a_1$ orbitals in MoS_4^{2-} and MoO_4^{2-}. In the case of MoS_4^{2-}, the amount of charge that develops on the central Mo ligand is 0.340e

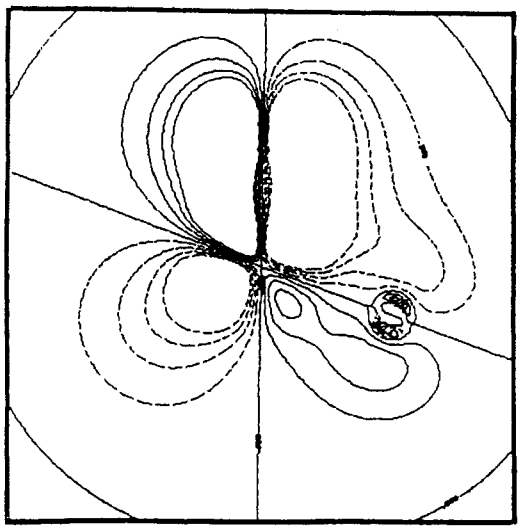

Figure 7. Contour map of the $1a_2$ orbital in $MoS_2O_2^{2-}$ that shows π-bonding interactions involving the $Mo(d_{xy})$ component and S and O ligands. The plotting plane is taken in a section that contains the Mo atom and the S and O ligands (Chart I). Increments of contour lines are the same as in Figure 2.

(1e), 0.398e ($2t_2$), and 0.193e ($2a_1$) as compared to 0.248e, 0.300e, and 0.160e, respectively, in the case of MoO_4^{2-}. The sulfur ligands are, therefore, better σ- and π-electron donors. The same conclusion may be obtained by calculating the charge (q_m) that develops on the central Mo atom as a result of the bonding scheme in the species under consideration. This charge may be computed by the formula

$$q_m = 42 - \left(q_m(\mathrm{SCF}) + \left[\frac{q(\mathrm{int}) + q(\mathrm{out})}{5} \right] \right)$$

where q_m(SCF) is the net charge on the Mo species after the attainment of an SCF potential and q(int) and q(out) are the charges in the inner- and outer-sphere regions, respectively. This charge is calculated to be +0.6e, +0.73e, +1.09e, +1.18e, and +1.57e in the species MoS_4^{2-}, MoS_3O^{2-}, $MoS_2O_2^{2-}$, $MoSO_3^{2-}$, and MoO_4^{2-}, respectively. Increasing the oxygen content in the species under consideration would lead to more ionic bond character. Although the net dipole moment in the tetrahedral species will be zero because of symmetry, one should still expect a gradual increase in the dipole moment along the series MoS_3O^{2-}, $MoS_2O_2^{2-}$, and $MoSO_3^{2-}$.

Consistent as they may appear, our results, however, seem to be at variance with LCAO–MO parameterized intensity calculations.[32] In the latter work, the authors reach the conclusion that the tetraoxo species are more π covalent that the corresponding tetrathio species. This conclusion is based on their result that the LUMO has predominantly metal atomic character in MoS_4^{2-} while it is an admixture of metal and ligand character in MoO_4^{2-}. This is not consistent with our results, which predict the metal character in the LUMO to increase successively as the number of oxygen ligands is increased. It is our contention that the sulfur ligands, being better electron donors (i.e. reductants) than the oxygen ligands, can participate in processes involving charge donation to the Mo atom via the 1e and $2t_2$ orbitals in a manner that will contribute to the covalency of the bonds. It is noteworthy to stress the fact that, in our model, the molybdenum is initially assumed to be in a d^0 configuration and that the amount of charge that develops on the Mo sphere in each of the different molecular orbitals must be in the form of charge back-donated from the ligands. These results are consistent with previous MS–Xα[33] and local density calculations.[34]

The results that have been presented so far agree well with MO calculations that were conducted on the tetraoxo and tetrathio species. The ordering of the levels is identical with that of reported MS–Xα calculations, although these calculations use the touching-sphere method in contrast to our overlapping-sphere approximation and the relativistic corrections used in defining the Hamiltonian of the system. Our results also agree with discrete variational calculations[35] but differ slightly from discrete variational Xα calculations[36] with respect to the position of the $2t_2$ and 1e levels in the case of the tetraoxo and tetrathio species. Kutzler et al.[33] have conducted relativistic Xα calculations using the touching-sphere and overlapping-sphere techniques on MoO_4^{2-}, $MoS_2O_2^{2-}$, and MoS_4^{2-}, and our results seem to be invariant with theirs, except perhaps for an insignificant difference in the ordering of the orbitals in the case of the dioxo dithio species, apparently due to a difference in the amount of sphere overlap. Gagarin[37] has reported scattered-wave calculations on MoO_4^{2-} by using a predefined stabilizing potential in the outer-sphere region. Gagarin's results, however, deviate from the now accepted results concerning the electronic structure of 4d transition-metal tetrahedral complexes. Bernholc and Stiefel[34] conducted local density calculations on MoS_4^{2-} and $Mo_3S_9^{2-}$, and our results are in very good quantitative and qualitative agreement with results they reported for the tetrathiomolybdenum species.

Our study is intended to be a comparative work, and toward that end, general trends in the electronic structural changes in the thiomolybdate species will be sought. According to our results, for the series $MoS_nO_{4-n}^{2-}$ (n = 4–0) in order of decreasing n, the following has been observed:

(1) The HOMO for all the species is of preponderant sulfur p character (the case of n = 0 is naturally redundant).

(2) Except for the case when n = 3, there is an increase in the HOMO–LUMO gap.

(3) In the LUMO, the Mo(d) character successively increases.

(4) The sum of the net charge acquired by the Mo atom in all the occupied valence levels successively decreases.

(5) The sum of the net charge on the d component of Mo in the 1e and $2t_2$ orbitals in T_d symmetry and the other orbitals that span the same representation in the lower symmetry species successively decreases.

(6) Because of the descent in symmetry, the absorption spectra will be most difficult to analyze in the case when n = 2. Moreover, and for similar reasons, the first ionizaation potential will not follow a well-defined pattern. In the case of the tetrathio and tetraoxo anions, the ionization potential spectra will increase in that order.

(7) There is an increase in the net charge on the Mo atom.

(8) The net ionic character increases.

(9) The amount of ligand to metal charge donation decreases.

Initially we were disturbed by the underestimated HOMO–LUMO gap in MoS_3O^{2-}, but this seemed to repeat itself in a study that we are now conducting on thiotungstate species. One argument that may be presented as an explanation of this unexpected behavior is that the trithiomolybdate anion is the only member in the thiomolybdate series that has pure sulfur p character in the HOMO. Admixtures of oxygen p bases in the other members of the series would probably play an important role in stabilizing the HOMO. It is perhaps due to this bonding interaction that the HOMO–LUMO gap is observed to increase along the series beyond the trithiomolybdate anion.

In Table IX we report the longest wavelength transition bands for the thiomolybdenum species in addition to other charge-transfer bands. The absorption spectrum of MoS_4^{2-} is well understood, and the first excitation energy agrees very well with the experimental assignment.[35] The value reported by Kutzler et al., however, is underestimated, perhaps because of the fact that they have calculated the transition energy by promoting $^1/_3$ rather than the normal $^1/_2$ electron to the 2e state. The second experimental

(32) Surana, S. S. L.; Tandon, S. P.; Nolte, W. O.; Müller, A. *Can. J. Spectrosc.* **1979**, *24*(1), 18.
(33) Kutzler, F. W.; Natoli, C. R.; Misemer, D. K.; Doniach, S.; Hodgson, K. O. *J. Chem. Phys.* **1980**, *73*(7), 3274.
(34) Bernholc, J.; Stiefel, E. I. *Inorg. Chem.* **1985**, *24*, 1323.
(35) Müller, A.; Diemann, E. *Chem. Phys. Lett.* **1971**, *9*, 369.
(36) Ziegler, T.; Rauk, A.; Baerends, E. J. *J. Chem. Phys.* **1976**, *16*, 209.
(37) Gagarin, S. G. *Kinet. Katal.* **1982**, *23*(3), 578.

Table IX. Transition-State Energies (in 10^3 cm^{-1}) for Various Excitations in the Different Molybdenum Species[a]

MoS_4^{2-}	MoS_3O^{2-}	$MoS_2O_2^{2-}$	$MoSO_3^{2-}$
$1t_1 \rightarrow 2e$	$1a_2 \rightarrow 6e$	$4b_1 \rightarrow 7a_1$	$5e \rightarrow 6e$
21.4 [35] (22.3)	21.5 [38] (19.5)	25.4 [39] (33.2)	25.4 [39] (35.4)
$3t_2 \rightarrow 2e$	$5a_1 \rightarrow 6e$	$6a_1 \rightarrow 7a_1$	$5a_1 \rightarrow 6e$
31.3 [34] (30.1)	(31.4)	(39.4)	(41.2)
$3t_2 \rightarrow 4t_2$	$5a_1 \rightarrow 6a_1$	$6a_1 \rightarrow 3a_2$	$5a_1 \rightarrow 6a_1$
41.2 [34] (44.2)	(46.6)	(49.4)	(52.2)
$2t_2 \rightarrow 2e$	$3a_1 \rightarrow 6e$	$3a_1 \rightarrow 7a_1$	$3a_1 \rightarrow 6e$
(40.8)	(73.3)	(68.4)	(66.8)

[a] After the transitions are given, the experimental values are shown (the reference number is given in brackets). Theoretical values ($X\alpha$) are given in parentheses.

absorption band occurs at 31.3×10^3 cm^{-1} and had been assigned to the $3t_2 \rightarrow 2e$ excitation, in good agreement with our calculated value at 30.1×10^3 cm^{-1}. The third experimental absorption band occurs at 41.2×10^3 cm^{-1} and is assigned to a promotion of an electron from the $3t_2$ to the $4t_2$ orbitals. This agrees with our assignment for the same band, which is calculated to be 44.2×10^3 cm^{-1}. The experimental longest wavelength absorption bands in the other thiomolybdenum species agree qualitatively with our results despite a quantitative difference. In the case of MoS_3O^{2-}, our value is underestimated (19.5×10^3 cm^{-1}) relative to the experimental value at 21.5×10^3 cm^{-1}.[38] We also note that, because of symmetry considerations, the short-wavelength absorption band that involves a charge transfer from an orbital that contains preponderant Mo(d) character (the 4e orbital) to the LUMO is a process that involves transfer of charge from the oxygen rather than the sulfur ligands.

In the dithio analogue, promotion of electrons to the $7a_1$ orbital is allowed from all levels except those that have a_2 symmetry, since such a promotion is a Laporte-forbidden transition of the type $^1A_2 \leftarrow {}^1A_1$. One therefore expects the first transition band to be a series of singlet excitations that represent charge transfer from the sulfur ligands to the Mo atom. This band is expected to be followed by another band that incorporates orbitals which have an admixture of Mo(d) and O(p) character and are therefore charge-transfer bands that involve the oxygen moieties. Unlike the other thiomolybdate species, the HOMO in the $MoSO_3^{2-}$ ion has E symmetry and the longest wavelength transition should correspond to a promotion of an electron from the 5e to the 6e orbitals. This results in having two allowed transitions to the $^1A_1$ and ^1E states and a forbidden transition to the $^1A_2$ state. The first allowed absorption band that involves charge transfer from the oxygen ligands corresponds to a promotion of an electron from the $1a_2$ to the 6e orbital ($^1E \leftarrow {}^1A_1$). The calculated first transition energies of the dithio- and monothiomolybdate species at 33.2×10^3 cm^{-1} and 35.4×10^3 cm^{-1}, respectively, are overestimated relative to the experimental assignment at 25.4×10^3 cm^{-1} for both transitions.[39] In spite of this rather poor correlation, one should observe that the experimental results give two distinct absorption bands. The first, which corresponds to the tetrathio and trithio species, occurs at $\simeq 21 \times 10^3$ cm^{-1}, while the second, which corresponds to the dithio and monothio species, occurs at $\simeq 25 \times 10^3$ cm^{-1}. This is exactly in line with the theoretical results that predict the first absorption bands to occur at an average of 20.9×10^3 cm^{-1} and the second to occur at an average of 34.3×10^3 cm^{-1}. We remind ourselves that the HOMO in the tetrathio and trithio species was found theoretically to be pure S(p) in character, in contrast to that for the dithio and monothio species, which was found to contain admixtures of S(p) (main contribution), O(p), and Mo(p) bases. We also report in Table IX other transition-state excitations in the thiomolybdate species that correspond to the $2t_2 \rightarrow 2e$ excitation in MoS_4^{2-}. As noted earlier, orbitals in the thiomolybdate species that correspond to the $2t_2$ orbital in MoS_4^{2-} are of preponderant O(p) character and the promotion of an electron from these respective orbitals to the LUMO should lead to an absorption band that would indicate the amount of oxygen ligands attached to the central Mo atom. In MoS_4^{2-}, for instance, the absorption peak that occurs at $\simeq 40 \times 10^3$ cm^{-1} will be expected to be gradually replaced by two peaks at shorter wavelengths as the oxygen ligand is made to replace a sulfur counterpart (one of the two new peaks according to our results corresponds to the $3a_1 \rightarrow 6e$ excitation and is found theoretically to be 73.3×10^3 cm^{-1}). Excitation energies that correspond to the promotion of an electron from the $3a_1$ orbitals in MoS_3O^{2-}, $MoS_2O_2^{2-}$, and MoS_3O^{2-} species to the respective LUMO's are henceforth reported in the table. All these excitations are charge-transfer processes that involve the O(p) bases and are, henceforth, larger than the $2t_2 \rightarrow 2e$ transition energy in MoS_4^{2-}. Note that the $3a_1$ orbitals in the trithio and monothio species constitute σ-bonding interactions between the $Mo(d_{z^2})$ component and the p_z bases of the O and S ligands, respectively.

Table X. MS $X\alpha$ Valence Ionization Energies (eV) of the Different Molybdenum Species

MoS_4^{2-}	MoS_3O^{2-}	$MoS_2O_2^{2-}$	$MoSO_3^{2-}$	MoO_4^{2-}
$1t_1$ (8.79)	$1a_2$ (8.53)	$4b_1$ (9.21)	5e (8.98)	$1t_1$ (11.20)
$3t_2$ (9.74)	5e (8.79)	$2a_2$ (9.42)	$5a_1$ (9.35)	$3t_2$ (11.60)
$2a_1$ (10.64)	$5a_1$ (10.34)	$4b_2$ (9.58)	$1a_2$ (9.66)	$2a_1$ (11.84)
1e (10.94)	4e (10.54)	$6a_1$ (10.01)	4e (9.90)	1e (13.66)
$2t_2$ (11.48)	$4a_1$ (10.59)	$3b_1$ (10.31)	$4a_1$ (11.22)	$2t_2$ (14.15)
$1t_2$ (19.40)	3e (11.24)	$5a_1$ (10.54)	3e (12.42)	$1t_2$ (26.08)
$1a_1$ (19.66)	2e (13.80)	$3b_2$ (11.41)	$3a_1$ (12.76)	$1a_1$ (26.32)
	$3a_1$ (15.93)	$2b_1$ (12.60)	2e (14.18)	
	1e (18.48)	$4a_1$ (12.93)	$2a_1$ (19.74)	
	$2a_1$ (19.97)	$1a_2$ (12.94)	$1a_1$ (25.55)	
	$1a_1$ (28.73)	$3a_1$ (14.27)	1e (25.99)	
		$2b_2$ (14.88)		
		$1b_1$ (19.60)		
		$2a_1$ (19.67)		
		$1b_2$ (26.84)		
		$1a_1$ (26.87)		

Finally we report in Table X a complete spectrum of ionization potentials (in eV) for the valence orbitals in the different molybdenum species by using the transition-state method of Slater.[31] Not much experimental work has been conducted in this particular area, and our data are mainly intended to be a reference for future work. We mention, however, a recent work by Liang et al.,[17] who have reported XPS data on, among others, the tetrathiomolybdenum species. The HOMO–LUMO gap reported by Liang et al. is 2.5 eV, which is very close to our calculated 2.49 eV. The first XPS valence spectrum appears as one band at $\simeq 2$ eV and is attributed to ionization from the $1t_1$ and $3t_2$ levels. The second XPS valence band spectrum is attributed to orbitals that originate from the Mo–S bonding states which involve the Mo(4d) and S(3p) bases (the 1e and $2t_2$ orbitals) and is reported to occur at approximately 4.5 eV. The difference between the two bands (Δ_{12}) is approximately 2 eV. This agrees very well with our calculated value of Δ_{12} of 1.98 eV, which may be obtained by taking the difference between the average value of the binding energies of the $1t_1$ and $3t_2$ states and the average of the binding energies of the 1e and $2t_2$ states. The difference between the second XPS band and the band that had been associated with the localized S(3s) bases is $\simeq 8.7$ eV, which compares quite well with our calculated value of 8.30 eV that may be obtained by taking the difference between the average of the binding energies of the 1e and $2t_2$ states and the average of the binding energies of the $1t_2$ and $1a_1$ states.

Acknowledgment. We express our gratitude to Dr. Y. Sawan of the Chemistry Department at Kuwait Univeristy for very fruitful discussions. Credit is also due to S. HafezAlsaheh and R. N. Budeir for technical help. We also acknowledge the Research Management Unit at the University of Kuwait for supporting this work (Research Grant SC033).

Registry No. MoS_4^{2-}, 16330-92-0; MoS_3O^{2-}, 19452-56-3; $MoS_2O_2^{2-}$, 16608-22-3; $MoSO_3^{2-}$, 25326-93-6; MoO_4^{2-}, 14259-85-9.

(38) Diemann, E.; Müller, A. *Spectrochim. Acta* **1970**, *A26*, 215.
(39) Müller, A.; Diemann, E.; Ranade, A. C.; Aymonino, P. J. *Z. Naturforsch.* **1969**, *B24*, 1247.